Electronic Supplementary Information

Benzothiadiazole-vinyl-linked POSS porous hybrid polymer enables photocatalytic oxidative coupling of amines in air

Yunjie Mao,† Jinfeng Yu,† Qing Shi, Xiaomeng Bai, Yulong Lin, Yifan Chen, Zhouyang Long* and Guojian Chen*

School of Chemistry and Materials Science, Jiangsu Key Laboratory of Green Synthetic Chemistry for Functional Materials, Jiangsu Normal University, Xuzhou, 221116, China.

* Corresponding authors, E-mail: gjchen@jsnu.edu.cn; longzhouyangfat@163.com

† These authors contributed equally to this work.

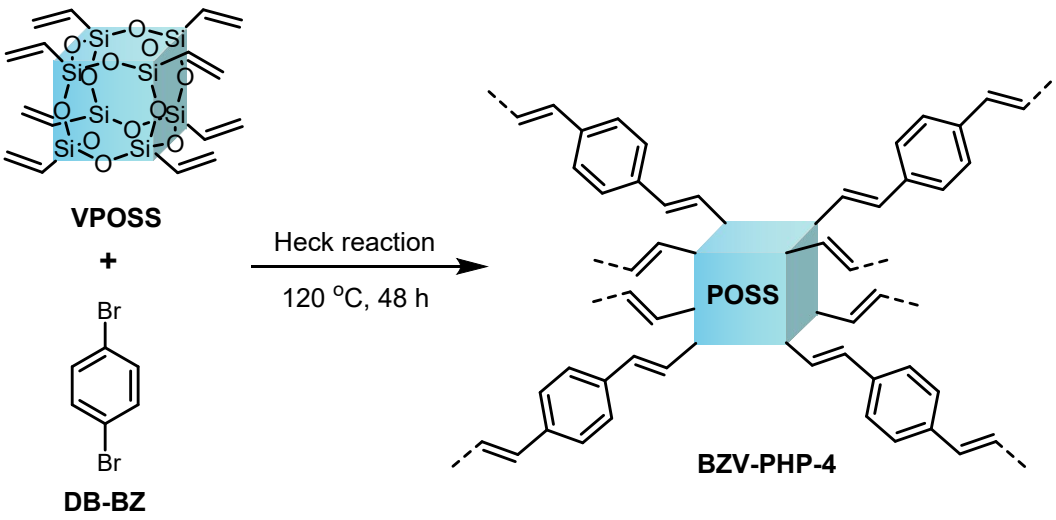

Scheme S1 Synthetic route to the benzene-vinyl-linked POSS porous hybrid polymer (BZV-PHP-4) by the Heck coupling reaction between octavinylsilsesquioxane (VPOSS) and 1,4-dibromobenzene (DB-BZ). Reaction conditions: *n*(VPOSS):*n*(DB-BZ)=1:4, $Pd(PPh_3)_4$, DMF, K_2CO_3, 120 ℃, 48 h.

Table S1 Porous textural parameters of BTV-PHP-*x* series.

Sample [a]	*n*(VPOSS): *n*(DB-BT)	S_{BET} [b] ($m^2\ g^{-1}$)	V_p [c] ($cm^3\ g^{-1}$)	S_{micro} [d] ($m^2\ g^{-1}$)	V_{micro} [d] ($cm^3\ g^{-1}$)	S_{micro}/S_{BET} (%)	V_{micro}/V_p (%)	D_p [e] (nm)
BTV-PHP-1	1:1	76	0.099	28	0.012	36.8	12.1	1.47, 3.97
BTV-PHP-2	1:2	279	0.464	107	0.049	38.4	10.6	1.47, 2.77
BTV-PHP-4	1:4	405	0.361	157	0.072	38.8	19.9	1.47, 3.79

[a] BTV-PHP-*x* polymers were obtained from the Heck reaction of VPOSS and DB-BT using different molar ratios (*x*=1, 2 and 4). [b] BET surface area (S_{BET}) calculated over the range P/P_0 = 0.05–0.20. [c] Total pore volume (V_p) calculated at P/P_0 = 0.99. [d] Micropore surface area (S_{micro}) and pore volume (V_{micro}) were calculated from the N_2 adsorption isotherm by the *t*-plot method. [e] The peak pore diameter (D_p) calculated by the NLDFT model.

Table S2 Comparisons of BET surface areas for BTV-PHP-4 and other related polymers including POSS-based porous polymers, and BT-containing COFs and POPs.

Entry	Sample	BET surface area ($m^2 g^{-1}$)	Ref.
0	BTV-PHP-4	405	This work
I.	**POSS-based porous polymers**		
1	OVS-Py-BT HPPs	354	S1
2	OVS-DBT-BT	386	S2
3	OVS-FO-POIP	264	S3
4	OVS-P-FHPP	375	S4
5	HPP1	358	S5
6	PCS-PSSP	287	S6
7	Bpy-PHP-4	384	S7
II.	**BT-containing COFs and POPs**		
8	Py-BSZ-COF	600	S8
9	BtCOF	340	S9
10	HIAM-0007	579	S10
11	HIAM-0018	467	S11
12	BTDA-TAPT	158.6	S12
13	hPorDTZ	386.8	S13
14	Pylm-B	558.82	S14

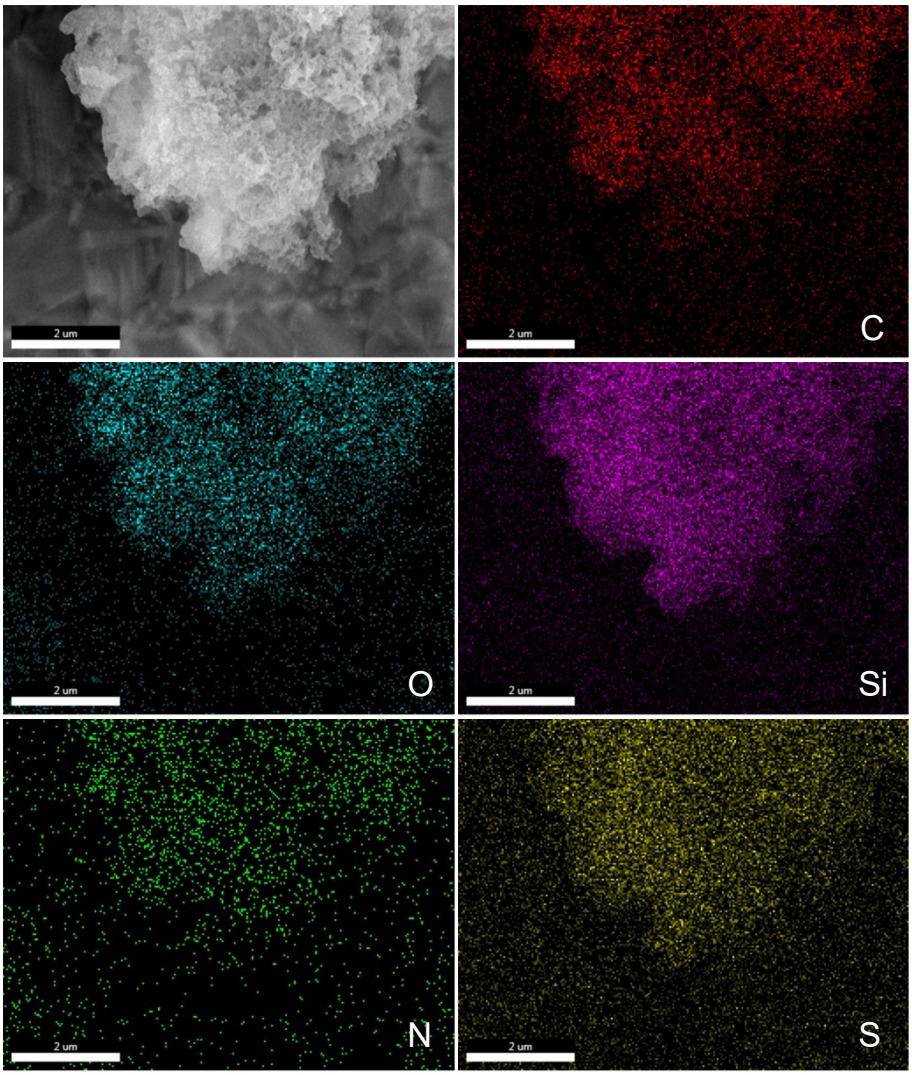

Fig. S1 SEM-EDS mapping images of C, O, Si, N, and S elements for the polymer BTV-PHP-4 (scale bar: 2 μm).

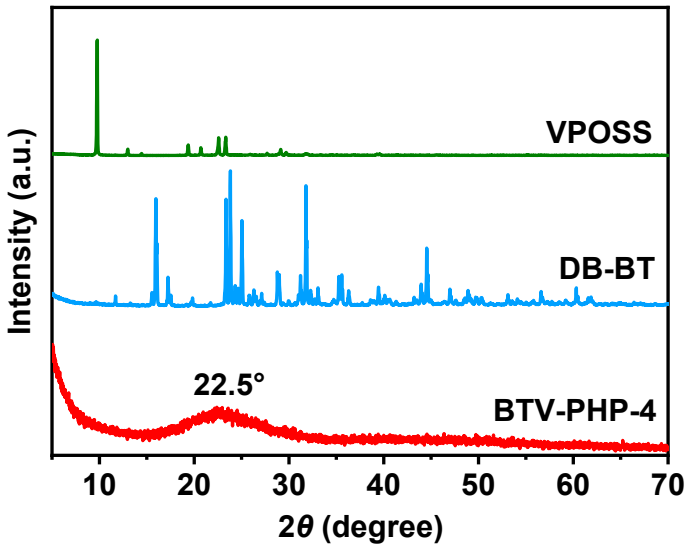

Fig. S2 XRD patterns of two building units VPOSS, DB-BT and the polymer BTV-PHP-4.

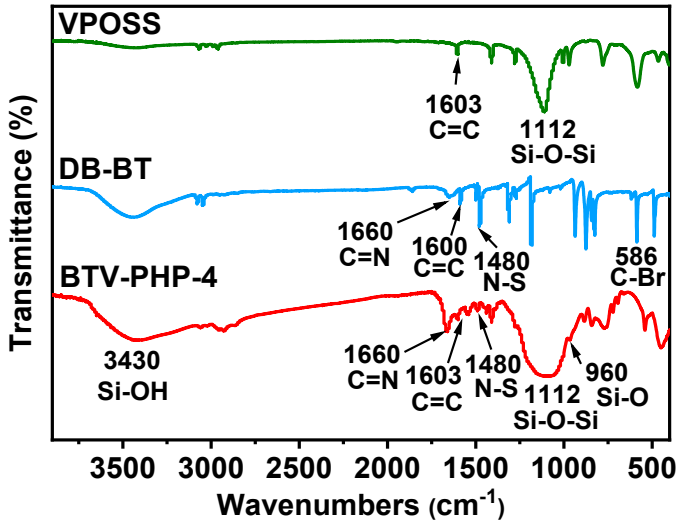

Fig. S3 FTIR spectra of VPOSS, DB-BT and BTV-PHP-4.

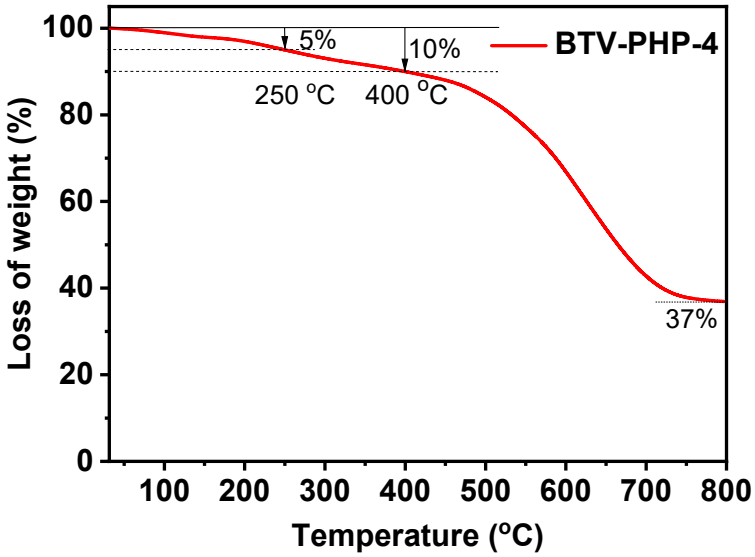

Fig. S4 Thermogravimetric analysis (TGA) curve of BTV-PHP-4 under air atmosphere.

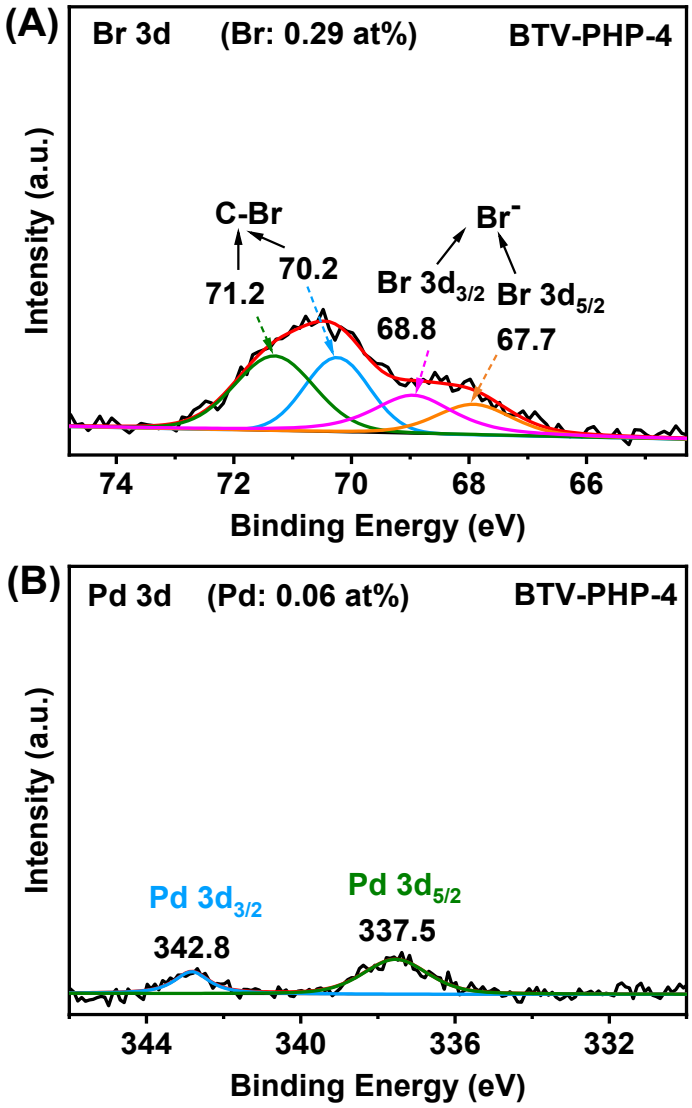

Fig. S5 XPS spectra of BTV-PHP-4: (A) Br 3d and (B) Pd 3d.

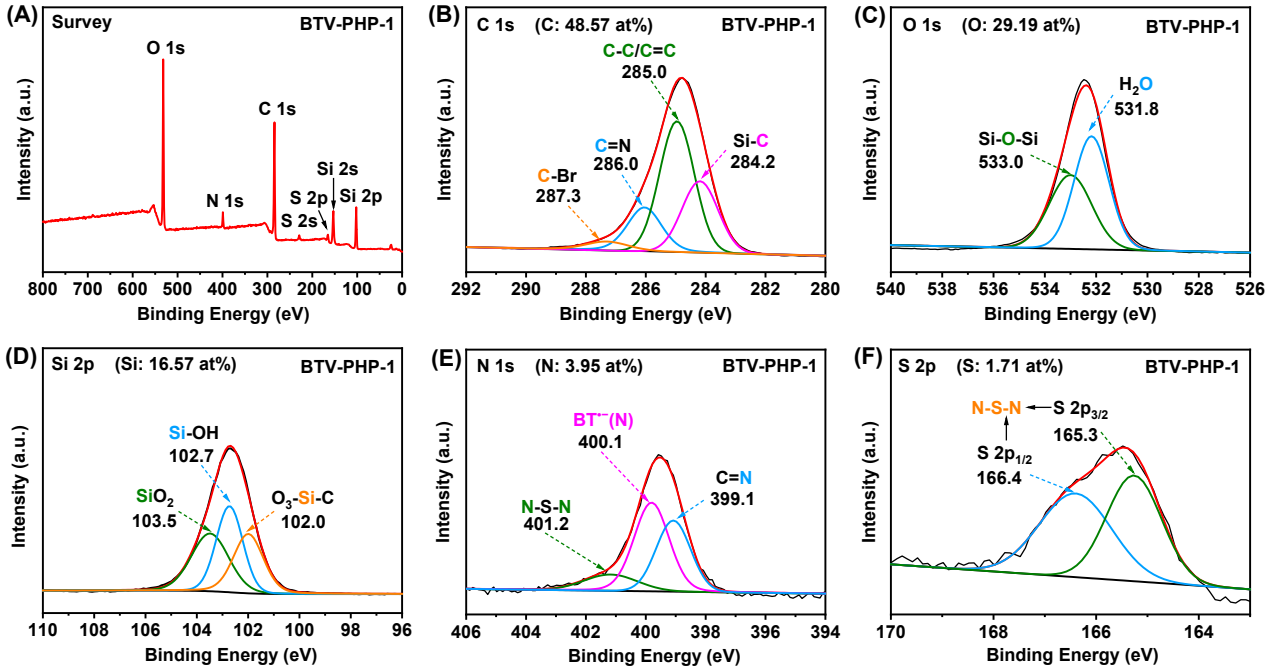

Fig. S6 XPS spectra of BTV-PHP-1: (A) survey, (B) C 1s, (C) O 1s, (D) Si 2p, (E) N 1s and (F) S 2p.

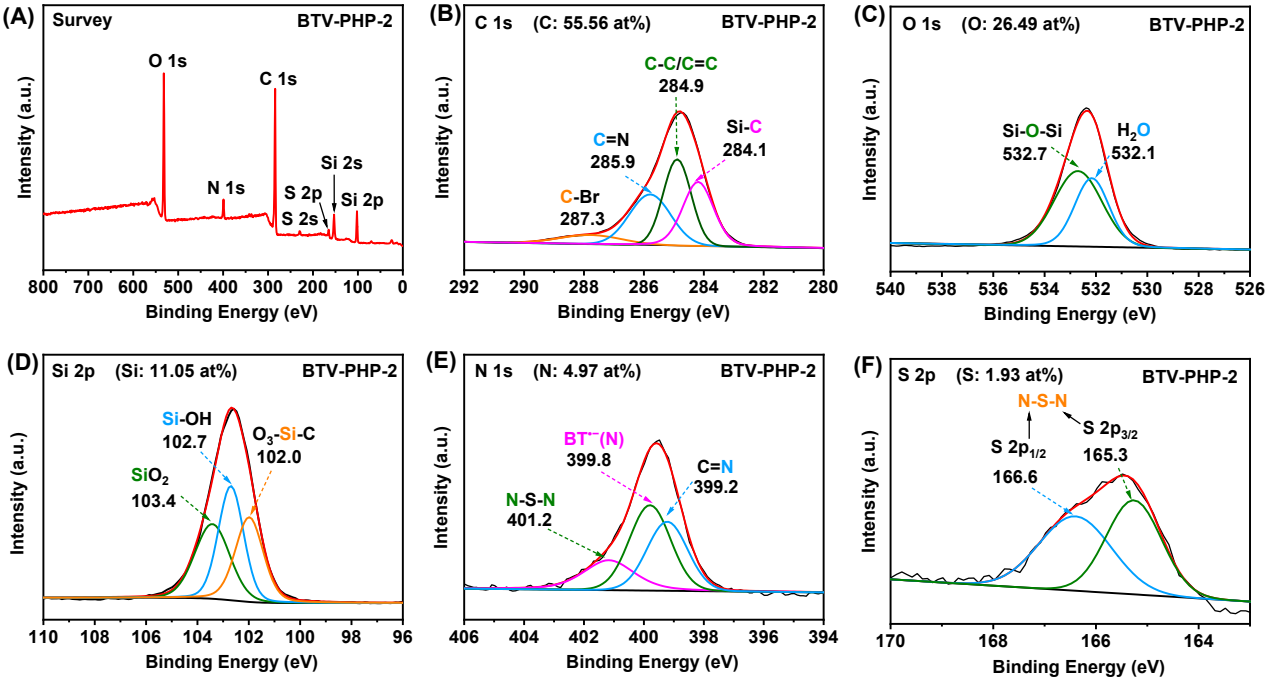

Fig. S7 XPS spectra of BTV-PHP-2: (A) survey, (B) C 1s, (C) O 1s, (D) Si 2p, (E) N 1s and (F) S 2p.

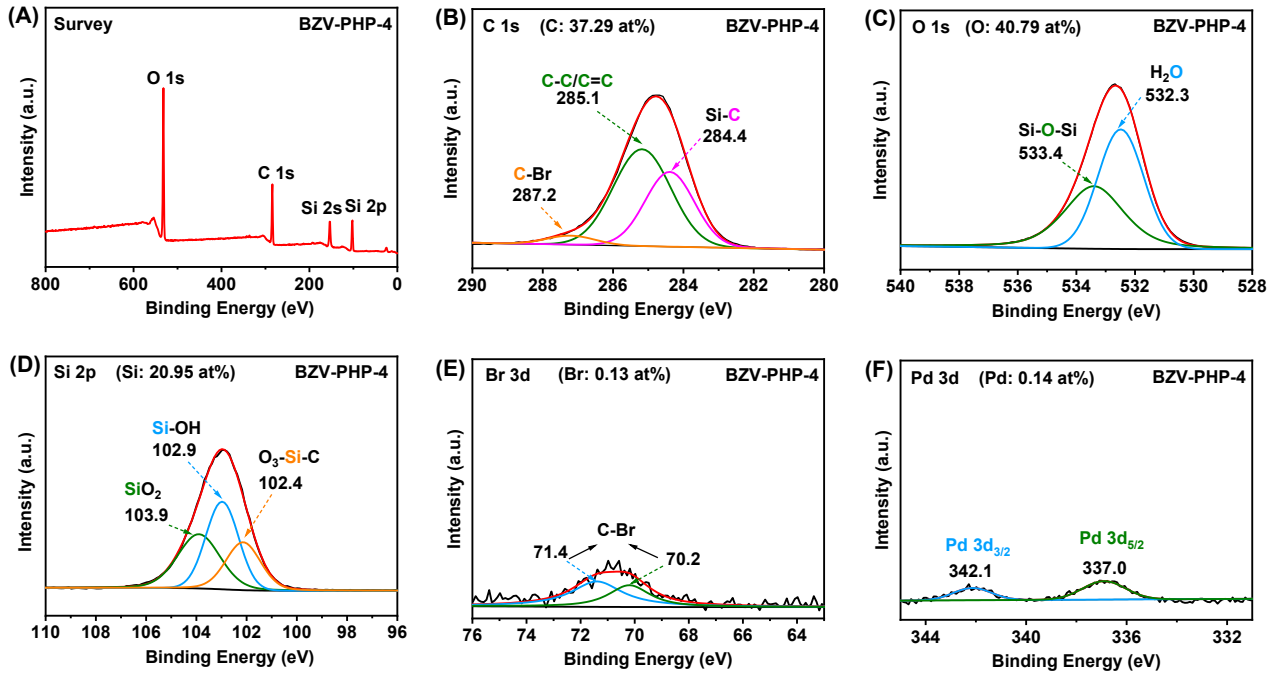

Fig. S8 XPS spectra of BZV-PHP-4: (A) survey, (B) C 1s, (C) O 1s, (D) Si 2p, (E) Br 3d, and (F) Pd 3d.

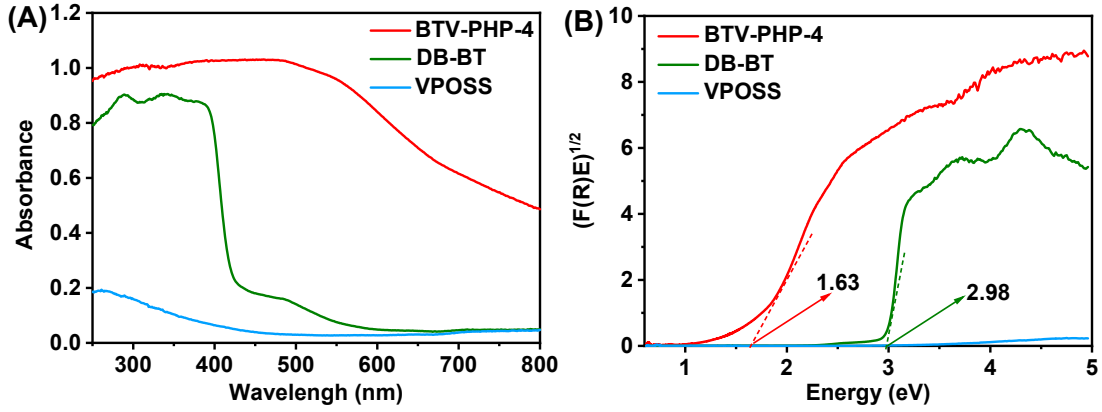

Fig. S9 (A) UV-Vis DRS of BTV-PHP-4, DB-BT and VPOSS, (B) Tauc plots calculated from the Kubelka–Munk function for obtaining optical bandgaps (E_g) of BTV-PHP-4 and DB-BT.

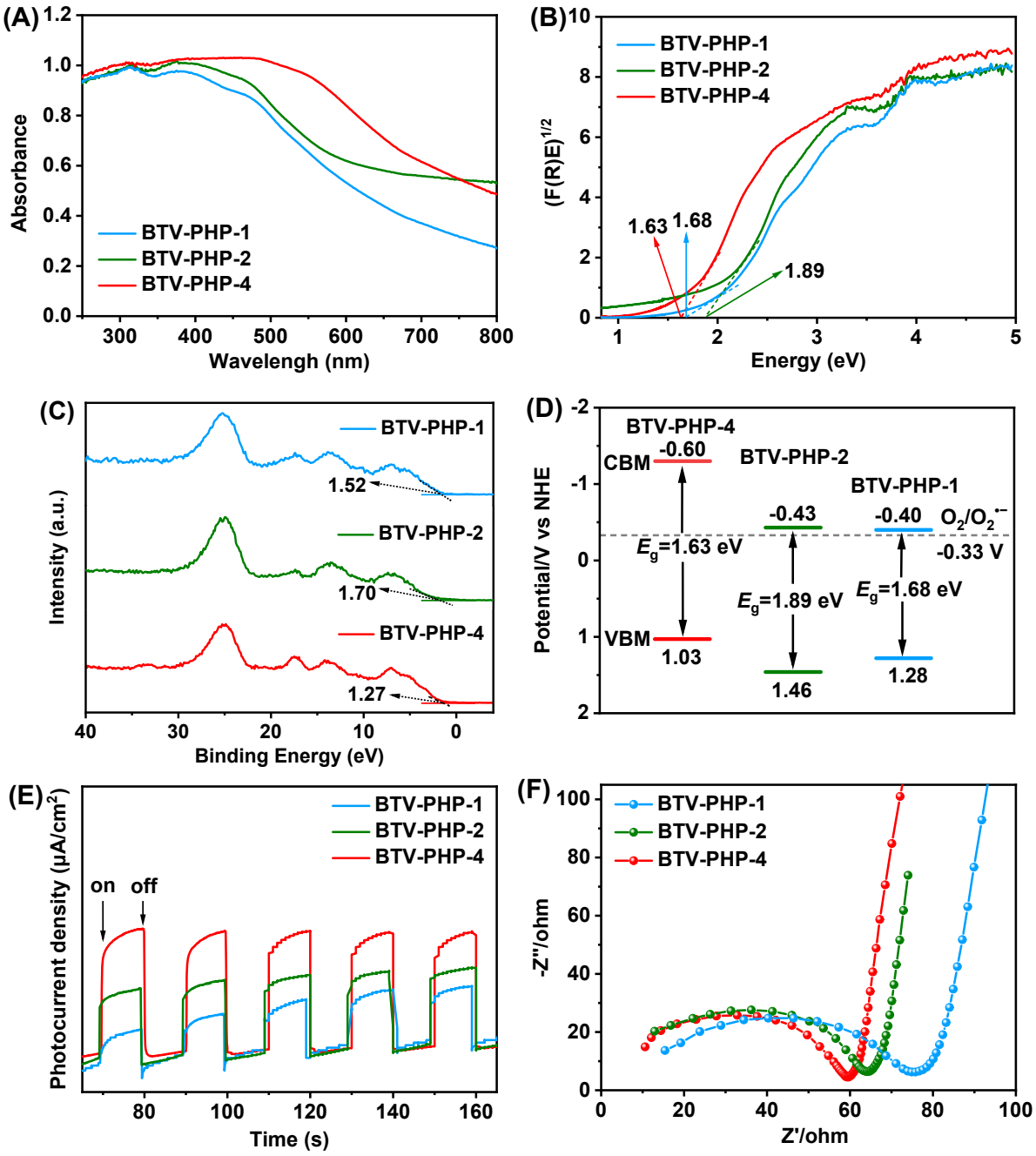

Fig. S10 (A) UV-Vis DRS and (B) Tauc plots calculated from the Kubelka-Munk function for optical bandgaps (E_g) of obtaining BTV-PHP-1, BTV-PHP-2 and BTV-PHP-4. (C) XPS VB spectra and (D) bandgap structures of BTV-PHP-1, BTV-PHP-2 and BTV-PHP-4. (E) Light on-of photocurrent responses and EIS Nyquist plots of BTV-PHP-1, BTV-PHP-2 and BTV-PHP-4.

Table S3 Comparisons for photocatalytic performance in the photocatalytic oxidative of benzylamine with O_2 or air at room temperature (RT) over COFs, POPs and porous organic salts (POSs) photocatalysts.

Entry	Photocatalyst	Reaction conditions	Solvent	Light source	*C* (%)	Ref.
0	BTV-PHP-4	Benzylamine (0.5 mmol), Cat. (5 mg), RT, air, 5 h	Solvent-free	Blue LEDs (5 W)	99	This work
I.	**Photocatalysts with benzothiadiazole structures**					
1	Py-BSZ-COF	Benzylamine (0.2 mmol), Cat. (5 mg), RT, air, 12 h	CH_3CN (2 mL)	LED (15 W, 520 nm, 5 mW cm^{-2})	99	S8
2	Ag/BTCOF	Benzylamine (1 mmol), Cat. (5 mg), RT, O_2, 4 h	CH_3CN (3 mL),	White LED light (λ > 400 nm)	90	S9
3	HIAM-0007	Benzylamine (0.3 mmol), Cat. (3 mg), RT, air, 24 h	CH_3CN (1 mL)	White LEDs	99	S10
4	HIAM-0020	Benzylamine (0.3 mmol), Cat. (3 mg), RT, air, 2 h	CH_3CN (1 mL)	White light (40 W)	99	S11
5	BTDA-TAPT	Benzylamine (0.1 mmol), Cat. (6 mg), RT, O_2, 6 h	CH_3CN (3 mL)	Xe lamp (300 W, λ = 420−780 nm)	97	S12
6	*h*PorDTZ	Benzylamine (1 mmol), Cat. (0.01 mmol), RT, air, 4 h	CH_3CN (1 mL)	Red light (640 nm, 1.2 mW cm^{-2})	99	S13
7	PY-BT COF	Benzylamine (0.1 mmol), Cat. (5 mg), RT, O_2, 2.5 h	CH_3CN (2 mL)	Xe-lamp (300 W)	99	S15
8	COF-BP	Benzylamine (0.1 mmol), Cat. (5 mg), RT, O_2, 5 h	CH_3CN (3 mL)	Xe lamp (300 W, λ = 420−780 nm)	98	S16

II.	**Other typical metal-free photocatalysts including COFs, POPs and POSs**					
9	AND-TAPT	Benzylamine (0.2 mmol), Cat. (5% mmol), RT, air, 24 h	CH_3CN (5 mL)	Blue LEDs (5 W)	99	S17
10	Vio-COF	Benzylamine (0.2 mmol), Cat. (2 μmol), 20 h	CH_3CN (2 mL)	Light (725 nm, 70 mW/cm^2)	99	S18
11	VCR-POP-1	Benzylamine (0.2 mmol), Cat. (3 mg), RT, air, 12 h	CH_3CN (2 mL)	White LEDs (5 W)	97	S19
12	NapTz-COF	Benzylamine (0.1 mmol), Cat. (5 mg), RT, O_2, 3 h	CH_3CN (2 mL)	Green LEDs (520 nm)	99	S20
13	BTT-Bpy-COF	Benzylamine (0.5 mmol), Cat. (10 mg),RT, O_2, 3 h	CH_3CN (3 mL)	LED light source (5 W*4, 465 nm)	99	S21
14	Tp-Tapb COF	Benzylamine (0.3 mmol), Cat. (5 mg), RT, air, 4.5 h	CH_3CN (2 mL)	Blue LEDs (16 W)	98	S22
15	TA-Por-sp^2-COF	Benzylamine (1 mmol), Cat. (5 mg), RT, air, 2 h	CH_3CN (20 mL)	White LEDs (15 W)	99	S23
16	aza-COF	Benzylamine (0.2 mmol), Cat. (10 mg), RT, O_2, 4 h	CH_3CN (3 mL)	LED (30 W, 365 nm)	96	S24
17	OML-4	Benzylamine (0.36 mmol), Cat. (8 mg), RT, air, 28 h	CH_3CN (2 mL)	Blue LED (12 W)	91	S25
18	NA-POS-1	Benzylamine (0.5 mmol), Cat. (5 mg), RT, air, 6 h	Solvent-free	Blue LEDs (5 W)	99	S26
19	VEY-PIS	Benzylamine (0.5 mmol), Cat. (5 mg), RT, air, 6 h	Solvent-free	Blue LEDs (5 W)	99	S27

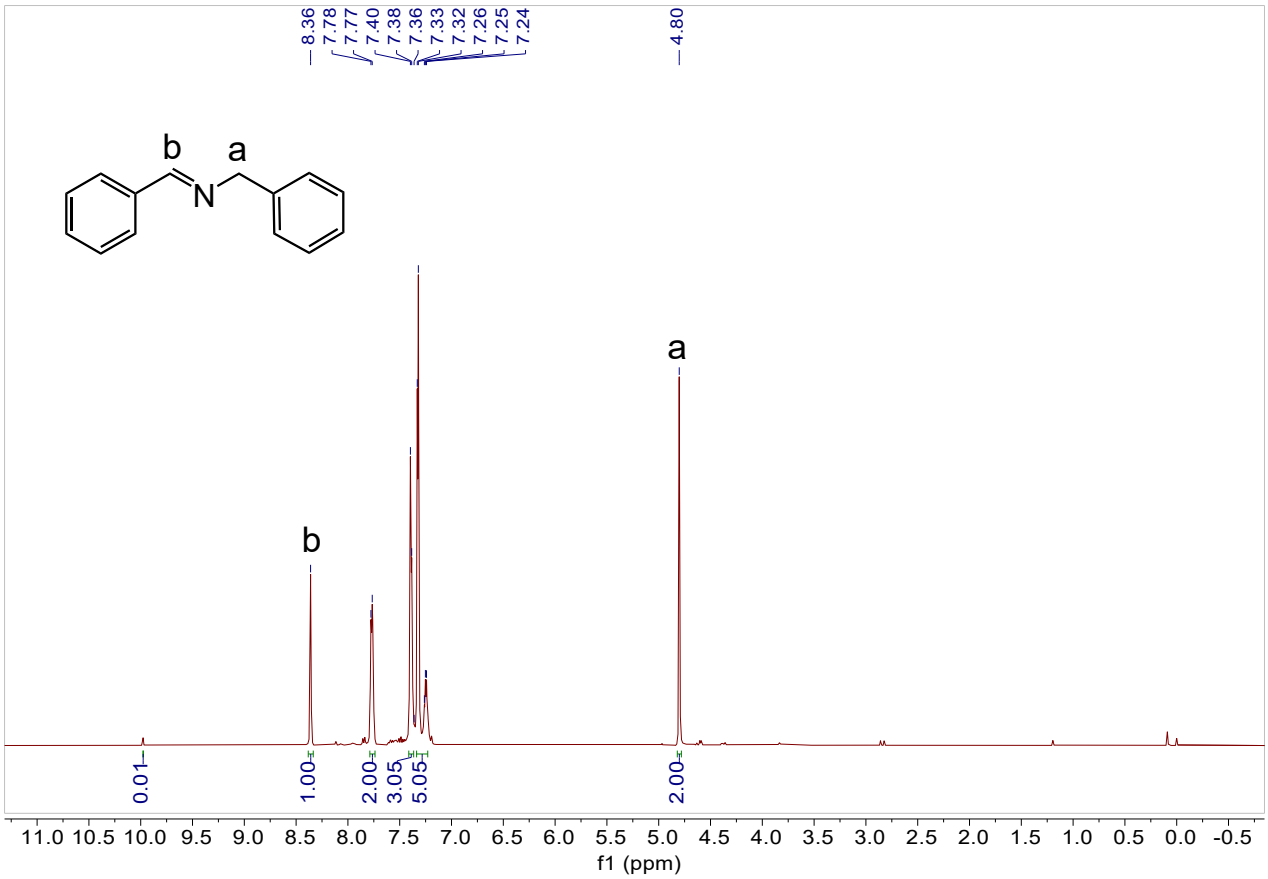

Fig. S11 ^{1}H NMR spectrum of *(E)*-N-benzyl-1-phenylmethanimine (**2a**) (400 MHz, $CDCl_3$): δ=8.36 (s, 1H), 7.78~7.77 (d, 2H), 7.40~7.36 (m, 3H), 7.33~7.24 (m, 5H) and 4.80 ppm (s, 2H). Reaction conditions: blue LEDs (5 W), room temperature, in air, 5 h, conversion of 99%, selectivity of 99%.

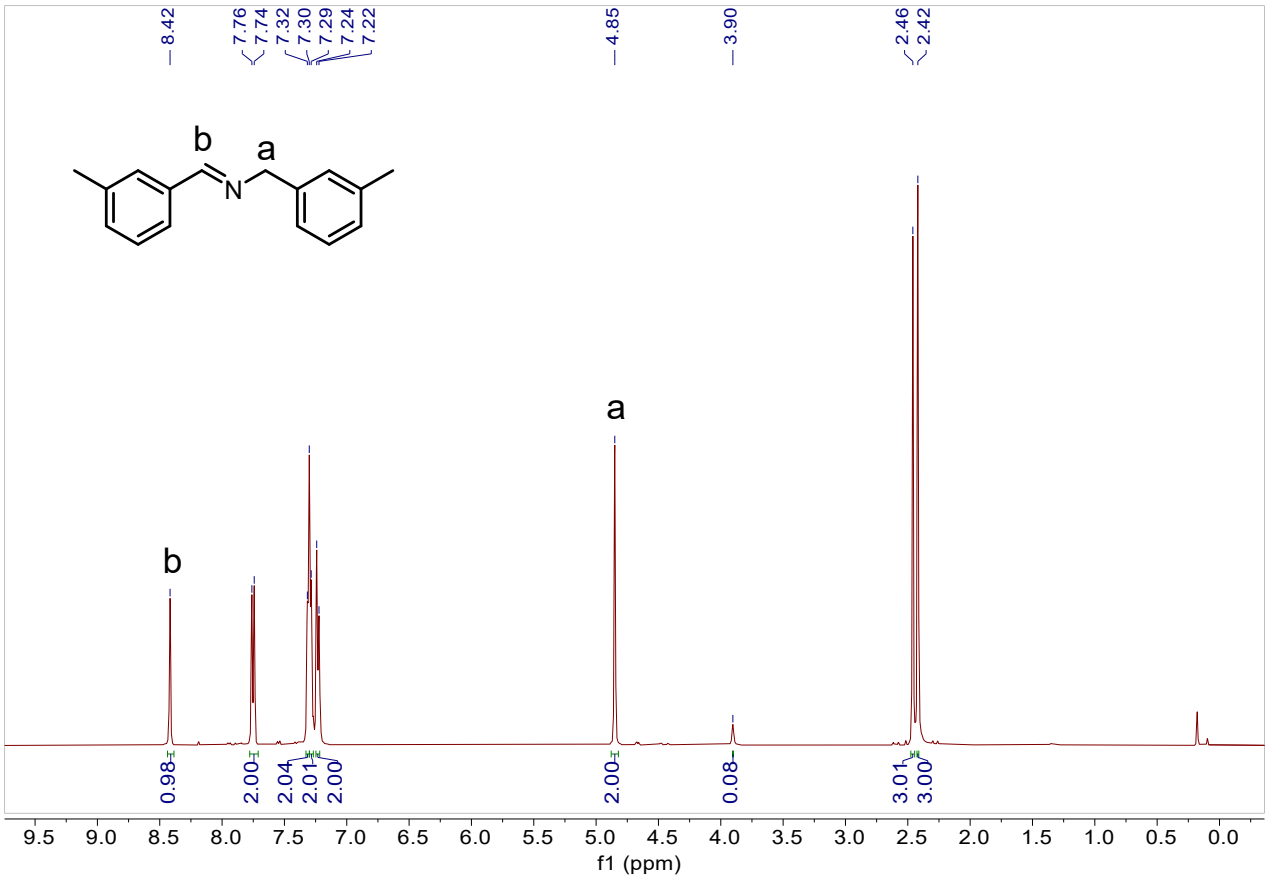

Fig. S12 ^{1}H NMR spectrum of *(E)*-N-(3-methylbenzyl)-1-(3-methylbenzyl)methanimine (**2b**) (400 MHz, $CDCl_3$): δ= 8.42 (s, 1H), 7.76~7.74 (d, 2H), 7.32~7.30 (d, 2H), 7.29~7.22 (m, 3H), 4.85 (s, 2H), 2.46 (s, 3H) and 2.42 ppm (s, 3H). Reaction conditions: blue LEDs (5 W), room temperature, in air, 4 h, conversion of 96%, selectivity of 99%.

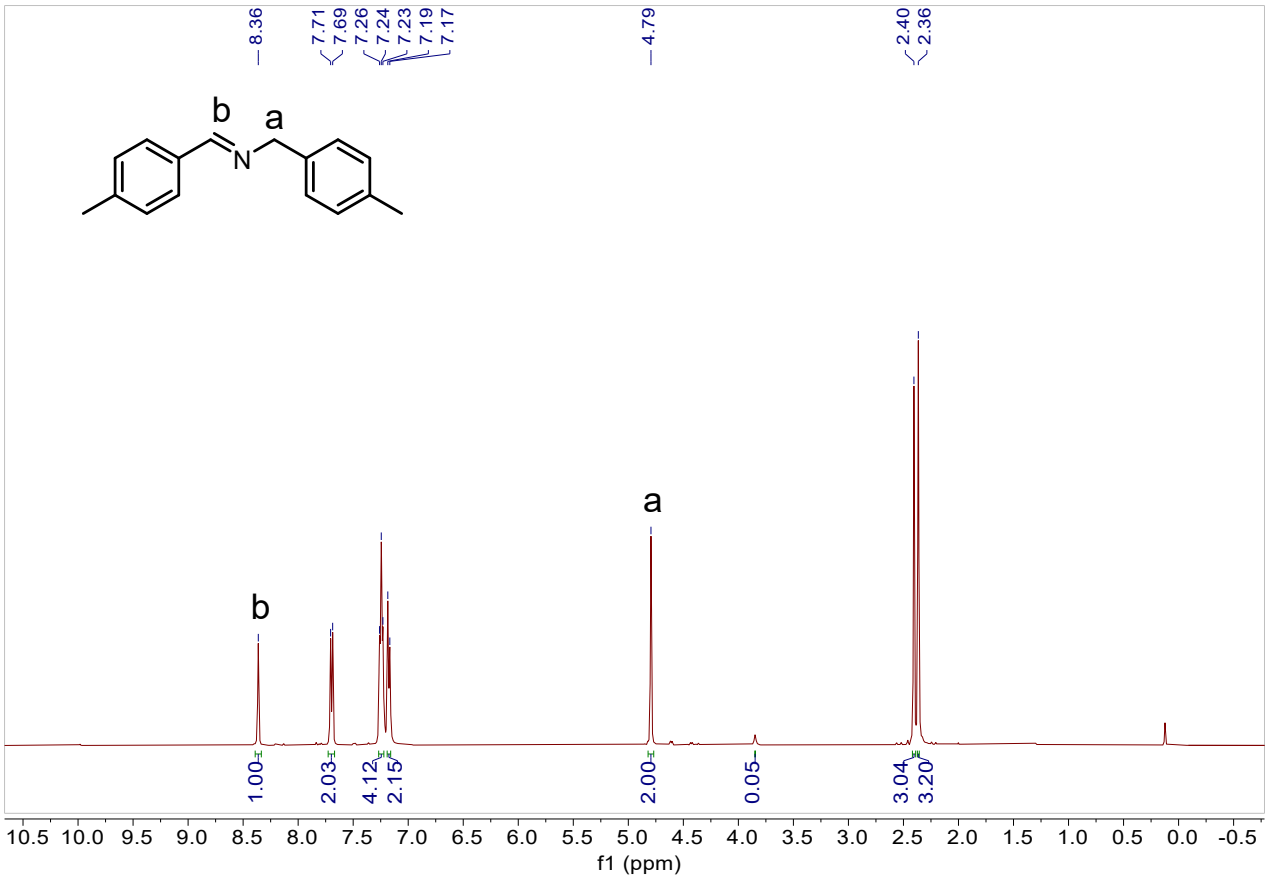

Fig. S13 ^{1}H NMR spectrum of *(E)*-N-(4-methylbenzyl)-1-(4-methylphenyl)methanimine (**2c**) (400 MHz, $CDCl_3$): δ=8.36 (s, 1H), 7.71~7.69 (d, 2H), 7.26~7.24 (d, 2H), 7.23~7.17 (m, 4H), 4.79 (s, 2H) and 2.40~2.36 ppm (d, 6H). Reaction conditions: blue LEDs (5 W), room temperature, in air, 6 h, conversion of 98%, selectivity of 99%.

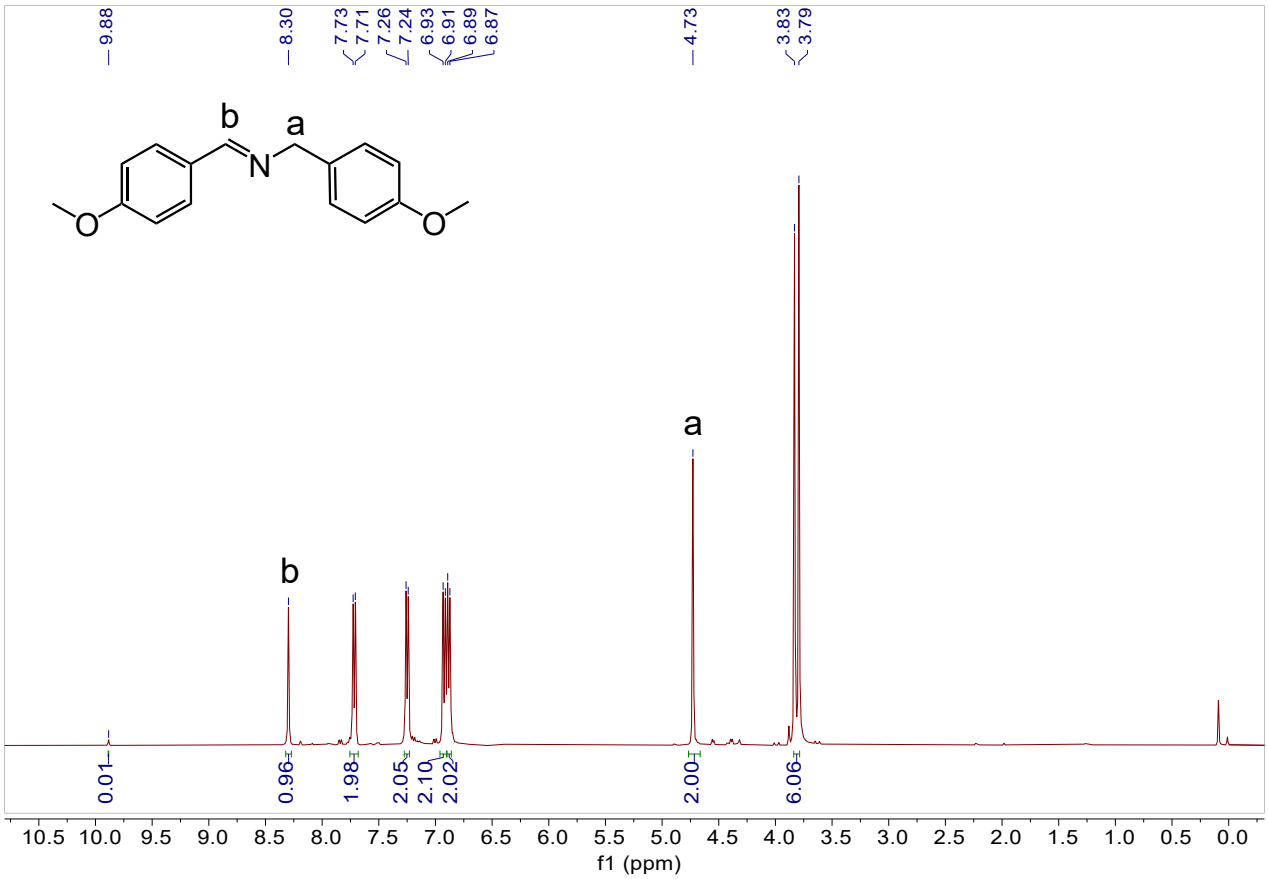

Fig. S14 ^{1}H NMR spectrum of *(E)*-N-(4-methoxybenzyl)-1-(4-methoxyphenyl)methanimine (**2d**) (400 MHz, $CDCl_3$): δ=8.30 (s, 1H), 7.73~7.31 (d, 2H), 7.26~7.24 (d, 2H), 6.93~6.91 (d, 2H), 6.89~6.87 (d, 2H), 4.73 (s, 2H) and 3.83~3.79 ppm (d, 6H). Reaction conditions: blue LEDs (5 W), room temperature, in air, 5 h, conversion of 99%, selectivity of 99%.

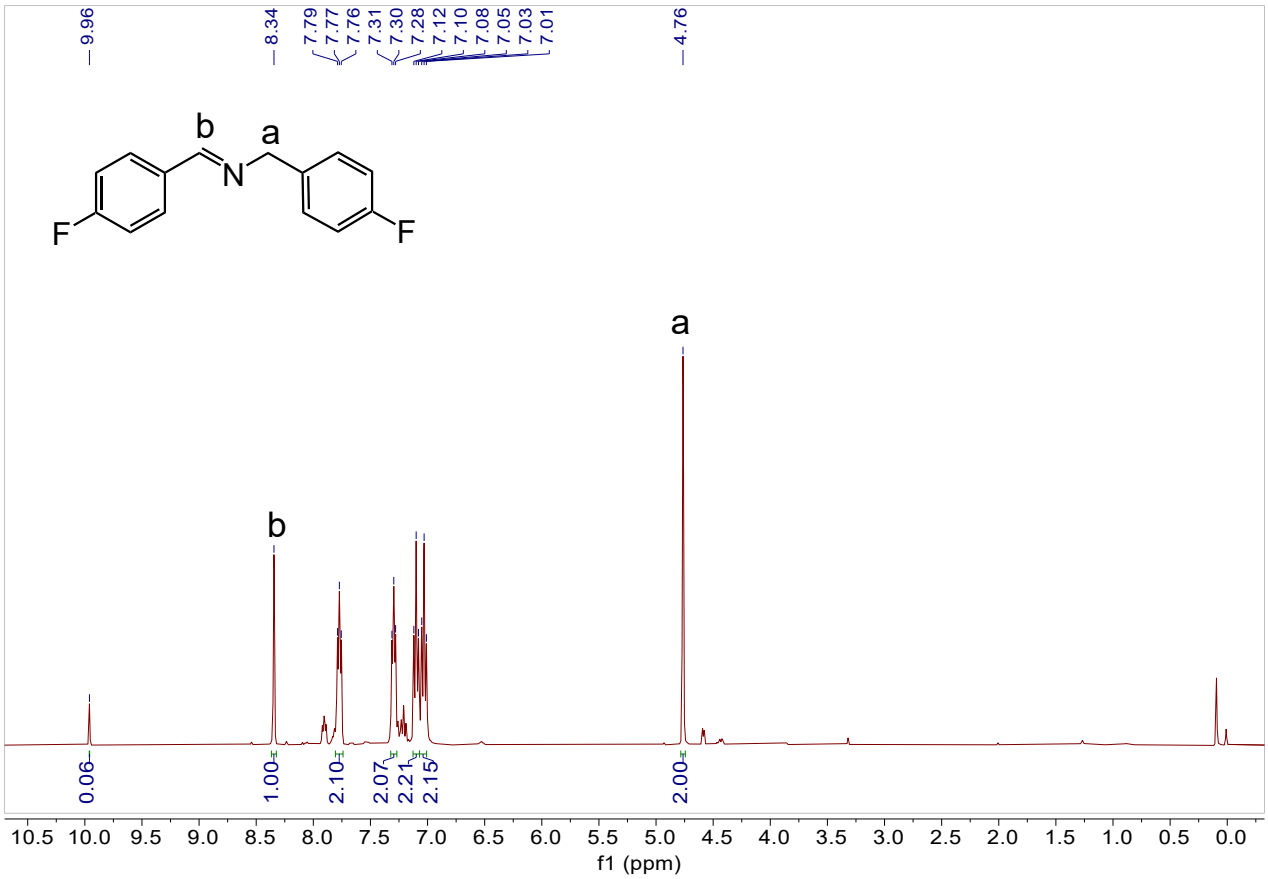

Fig. S15 ^{1}H NMR spectrum of *(E)*-N-(4-fluorobenzyl)-1-(4-fluorophenyl)methanimine (**2e**) (400 MHz, $CDCl_3$): δ= 8.34 (s, 1H), 7.79~7.76 (m, 2H), 7.31~7.28 (m, 2H), 7.10~7.01 (m, 4H) and 4.76 ppm (s, 2H). Reaction conditions: blue LEDs (5 W), room temperature, in air, 5 h, conversion of 99%, selectivity of 97%.

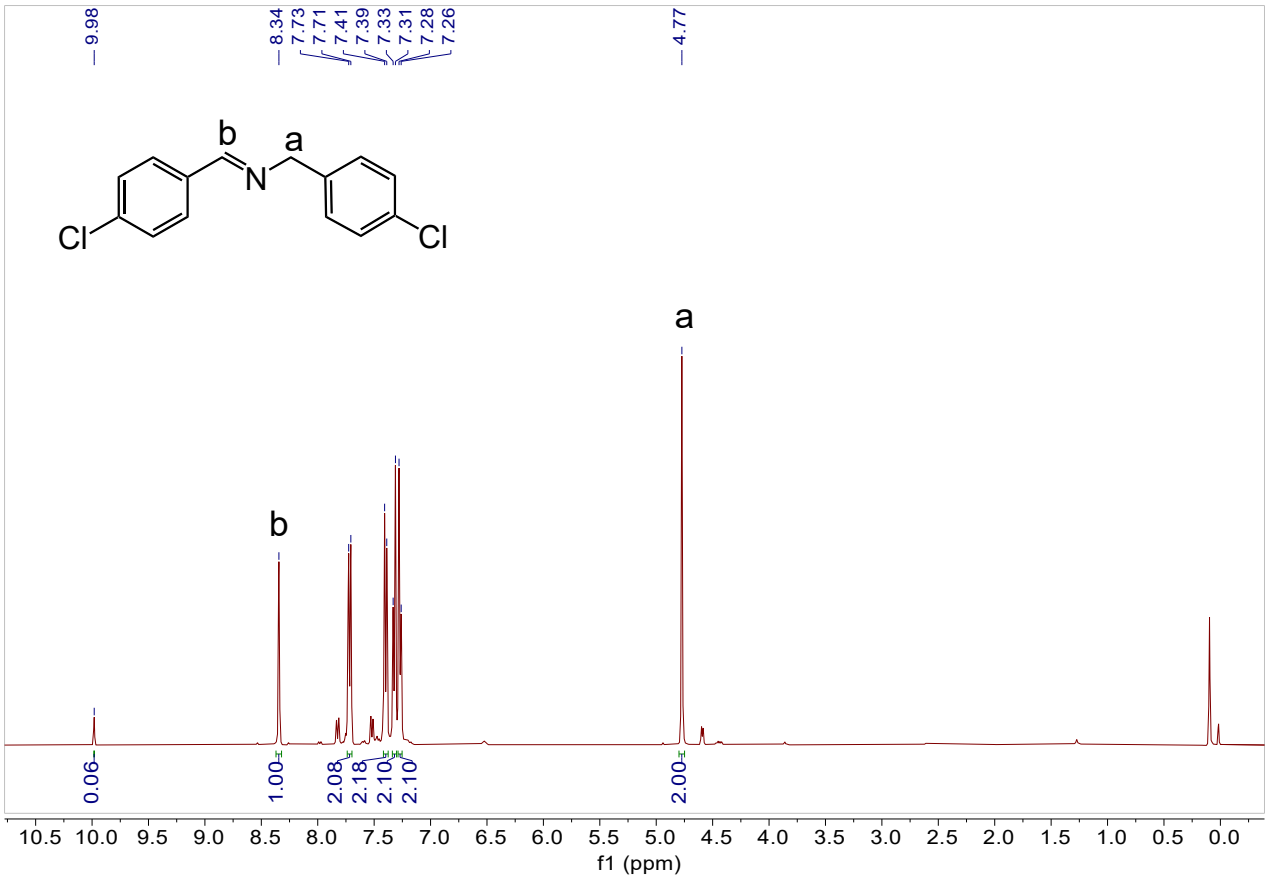

Fig. S16 ^{1}H NMR spectrum of *(E)*-N-(4-chlorobenzyl)-1-(4-chlorophenyl)methanimine (**2f**) (400 MHz, $CDCl_3$): δ= 8.34 (s, 1H), 7.73~7.71 (d, 2H), 7.41~7.39 (d, 2H), 7.33~7.31 (d, 2H), 7.28~7.26 (d, 2H) and 4.77 ppm (s, 2H). Reaction conditions: blue LEDs (5 W), room temperature, in air, 5 h, conversion of 99%, selectivity of 97%.

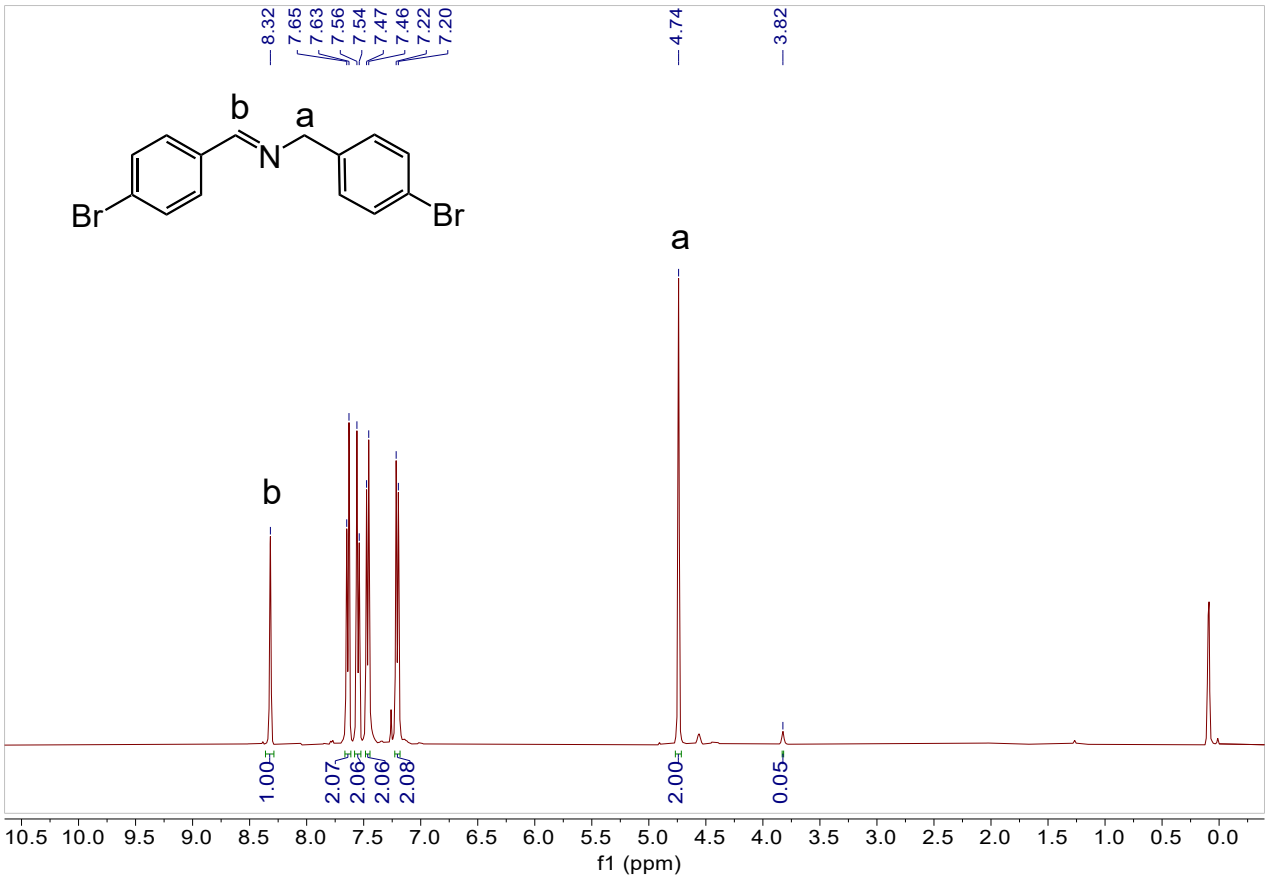

Fig. S17 ^{1}H NMR spectrum of *(E)*-N-(4-bromobenzyl)-1-(4-bromophenyl)methanimine (**2g**) (400 MHz, $CDCl_3$) : δ= 8.32 (s, 1H), 7.65~7.63 (d, 2H), 7.56~7.54 (d, 2H), 7.47~7.46 (d, 2H), 7.22~7.20 (d, 2H) and 4.74 ppm (s, 2H). Reaction conditions: blue LEDs (5 W), room temperature, in air, 7 h, conversion of 98%, selectivity of 99%.

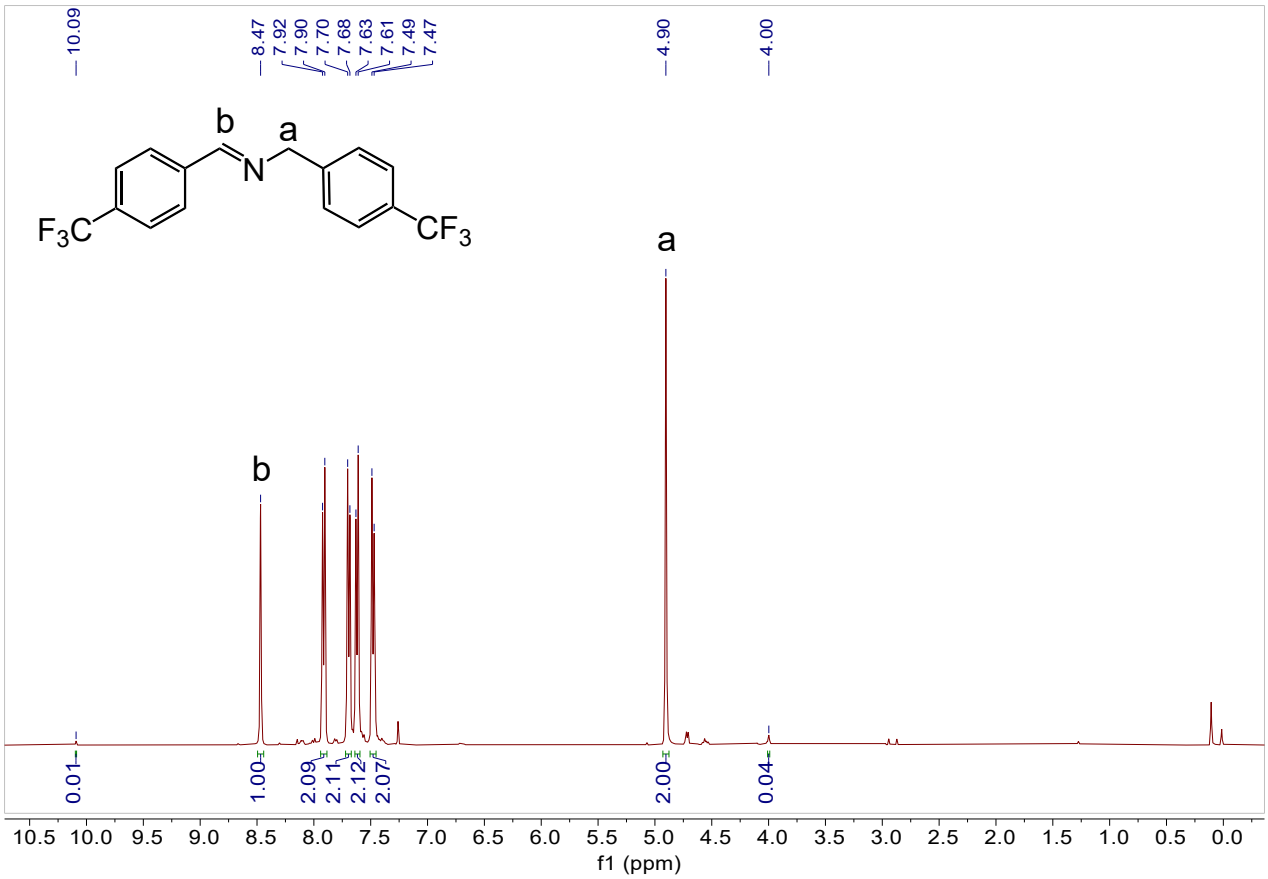

Fig. S18 ^{1}H NMR spectrum of *(E)*-N-(4-trifluoromethylbenzyl)-1-(4-trifluoromethylphenyl)methanimine (**2h**) (400 MHz, $CDCl_3$): δ=8.47 (s, 1H), 7.92~7.90 (d, 2H), 7.70~7.68 (d, 2H), 7.63~7.61 (d, 2H), 7.49~7.47 (d, 2H) and 4.90 ppm (s, 2H). Reaction conditions: blue LEDs (5 W), room temperature, in air, 6 h, conversion of 98%, selectivity of 99%.

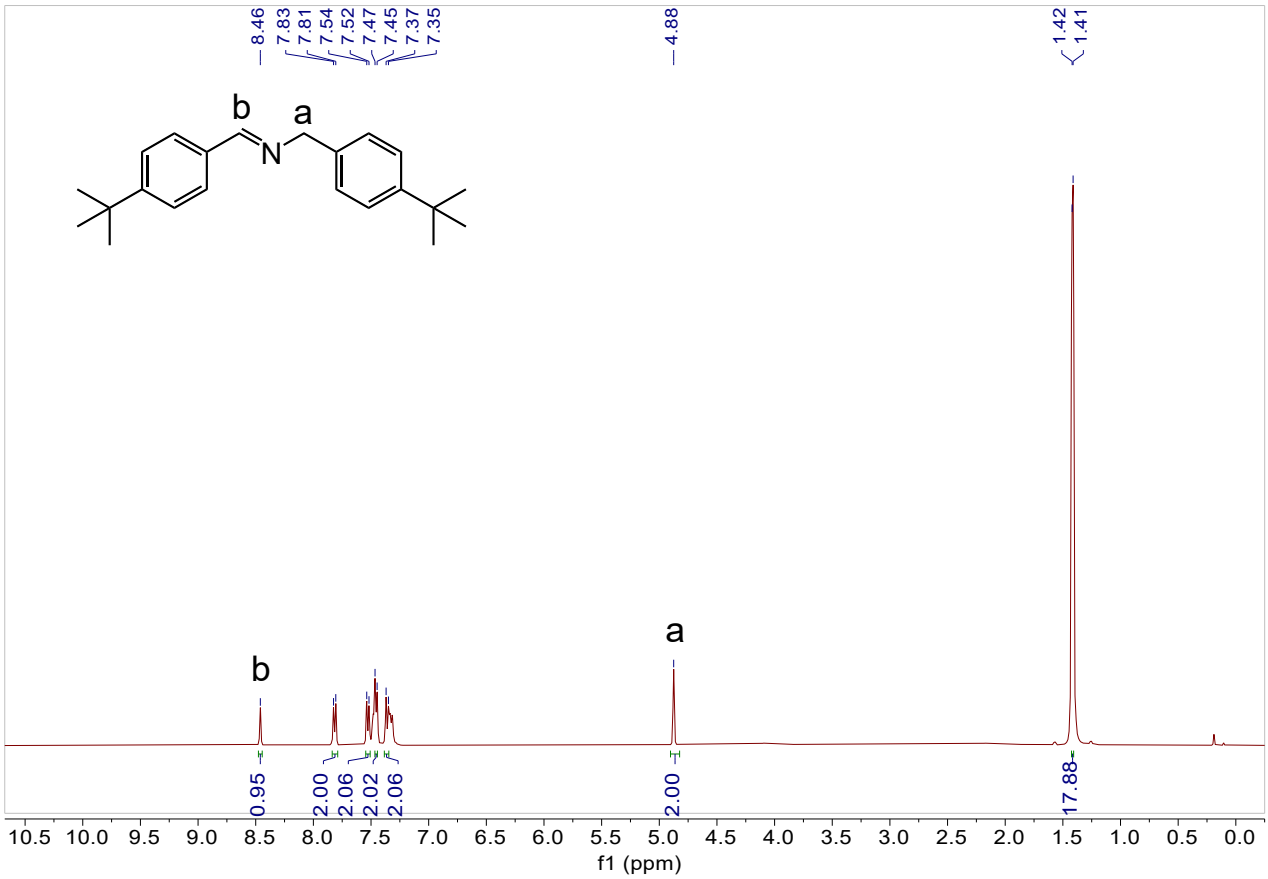

Fig. S19 ^{1}H NMR spectrum of *(E)*-N-(4-(tert-butyl)benzyl)-1-(4-(tert-butyl)phenyl)methanimine (**2i**) (400 MHz, $CDCl_3$): δ=8.46 (s, 1H), 7.83~7.81 (d, 2H), 7.54~7.52 (d, 2H), 7.47~7.45 (d, 2H), 7.37~7.35 (d, 2H), 4.88 (s, 2H) and 1.42~1.41 ppm (d, 18H). Reaction conditions: blue LEDs (5 W), room temperature, in air, 6 h, conversion of 99%, selectivity of 99%.

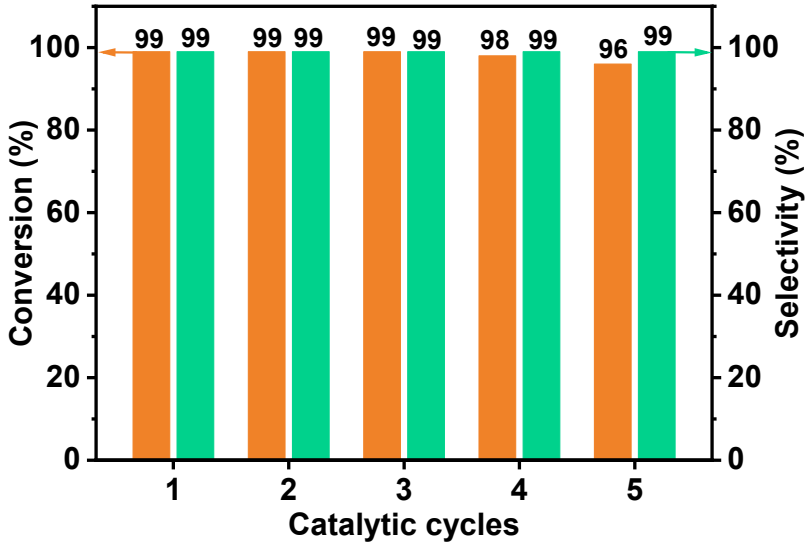

Fig. S20 Catalytic reusability of the photocatalyst BTV-PHP-4 in the solvent-free photocatalytic oxidative coupling of benzylamine. Reaction conditions: benzylamine (0.5 mmol), BTV-PHP-4 (5 mg), blue LEDs (5 W), in air, room temperature, 5 h.

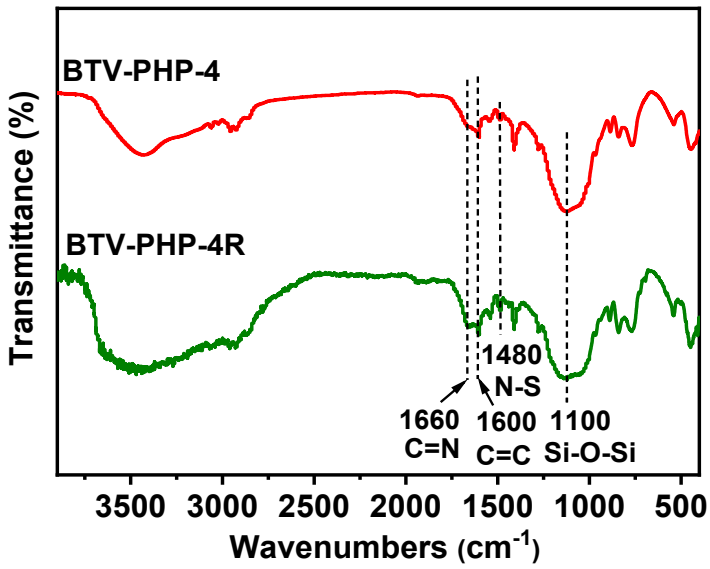

Fig. S21 FTIR spectra of the fresh photocatalyst BTV-PHP-4 and the recovered photocatalyst BTV-PHP-4R.

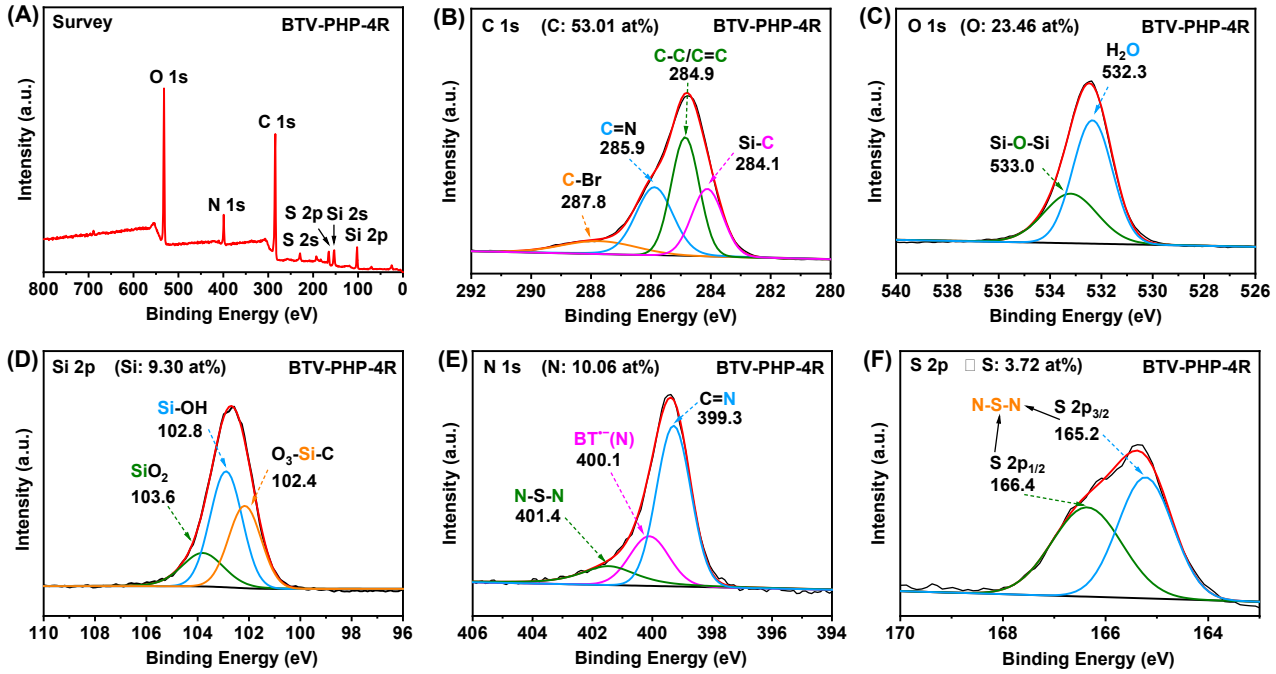

Fig. S22 XPS spectra of the recovered photocatalyst BTV-PHP-4R: (A) survey, (B) C 1s, (C) O 1s, (D) Si 2p, (E) N 1s, and (F) S 2p.

Potential chemical alterations, such as degradation of BT units or surface oxidation, were probed using FTIR and XPS spectroscopy. The FTIR spectrum of BTV-PHP-4R (Fig. S21) retains all characteristic bands of the fresh BTV-PHP-4. Crucially, the signals corresponding to the BT unit (*e.g.*, C=N, N-S) and the Si-O-Si framework remain unchanged, confirming the good chemical stability of both the photoactive BT unit and POSS cage. High-resolution XPS spectra (Fig. S22) further show that the binding energies and peak shapes for C 1s, O 1s, Si 2p, N 1s, and S 2p core levels are nearly identical to those of the fresh catalyst, with no new peaks indicative of significant oxidation (*e.g.*, new C=O or S=O species). The elemental compositions (C, O, Si, N, and S, Fig. S22) of BTV-PHP-4R also remains similar to those of BTV-PHP-4.

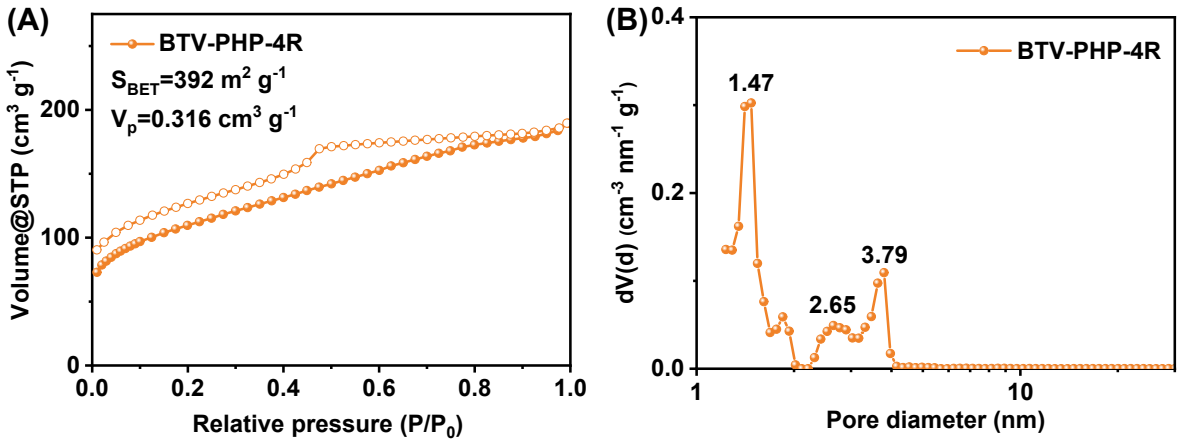

Fig. S23 (A) N_2 adsorption-desorption isotherms and (B) the pore size distribution calculated by the NLDFT method of the recovered photocatalyst BTV-PHP-4R.

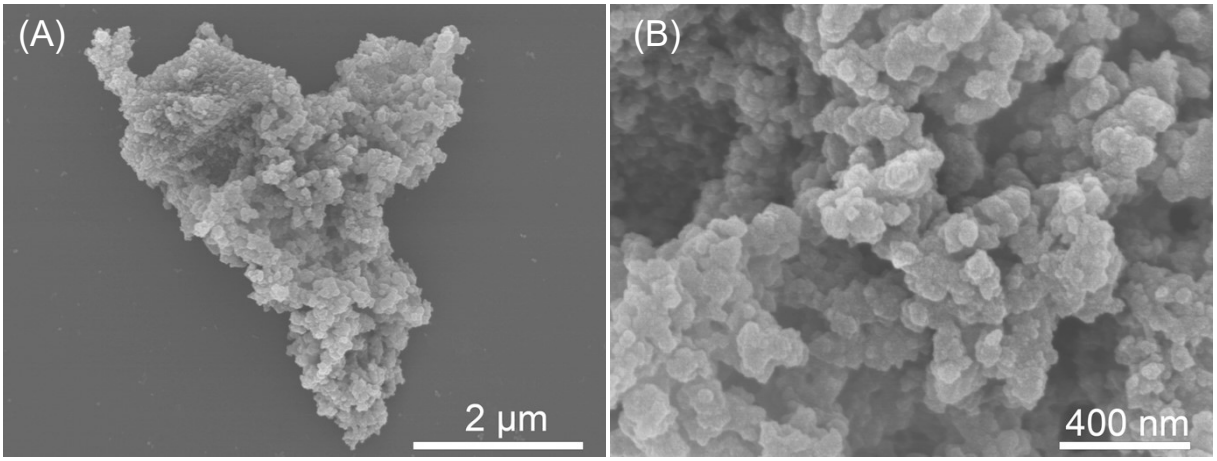

Fig. S24 SEM images of the recovered photocatalyst BTV-PHP-4R.

To evaluate potential physical changes such as pore blockage or particle aggregation after recycling, N_2 sorption analysis and SEM were performed on the recovered catalyst BTV-PHP-4R. The N_2 sorption isotherms (Fig. S23) show that BTV-PHP-4R retains a high BET surface area (~392 m^2 g^{-1}, compared to 405 m^2 g^{-1} for the fresh BTV-PHP-4) and a nearly identical pore size distribution. The slight decrease in surface area can be attributed to some adsorbed products within the catalyst, indicating negligible pore blockage. SEM images (Fig. S24) confirm that the characteristic fluffy nanoparticle morphology is well preserved, with no observable large-scale aggregation or significant change in particle size. These results demonstrate that no significant physical changes (pore blockage or particle aggregation) occurred during cycling, attributable to the robust 3D hybrid framework of BTV-PHP-4.

Table S4 Quenching experiments to assess the role of key reactive oxygen species (ROS) over the photocatalyst BTV-PHP-4.[a]

Entry	Scavenger	Role	*C* (%)[b]	*S* (%)[b]
1	-	Standard conditions	99	99
2	*p*-BQ [c]	$O_2^{\bullet-}$ scavenger	23	99
3	NaN_3 [d]	$^1O_2$ scavenger	16	99
5	$AgNO_3$ [e]	e^- trapper	3	99
6	KI [f]	h^+ trapper	21	99
7	*t*-BuOH	$^{\bullet}OH$ scavenger	99	99

[a] Standard reaction conditions: benzylamine (0.5 mmol), BTV-PHP-4 (5 mg), blue LEDs (5W), solvent-free, room temperature, in air, 5 h. [b] The conversion *(C)* and selectivity (*S*) were determined by ^1H NMR analyses. [c] *p*-BQ (*p*-benzoquinone) (0.5 mmol), [d] NaN_3 (0.25 mmol), [e] $AgNO_3$ (0.25 mmol), [f] KI (0.25 mmol) and [e] *t*-BuOH (0.25 mmol).

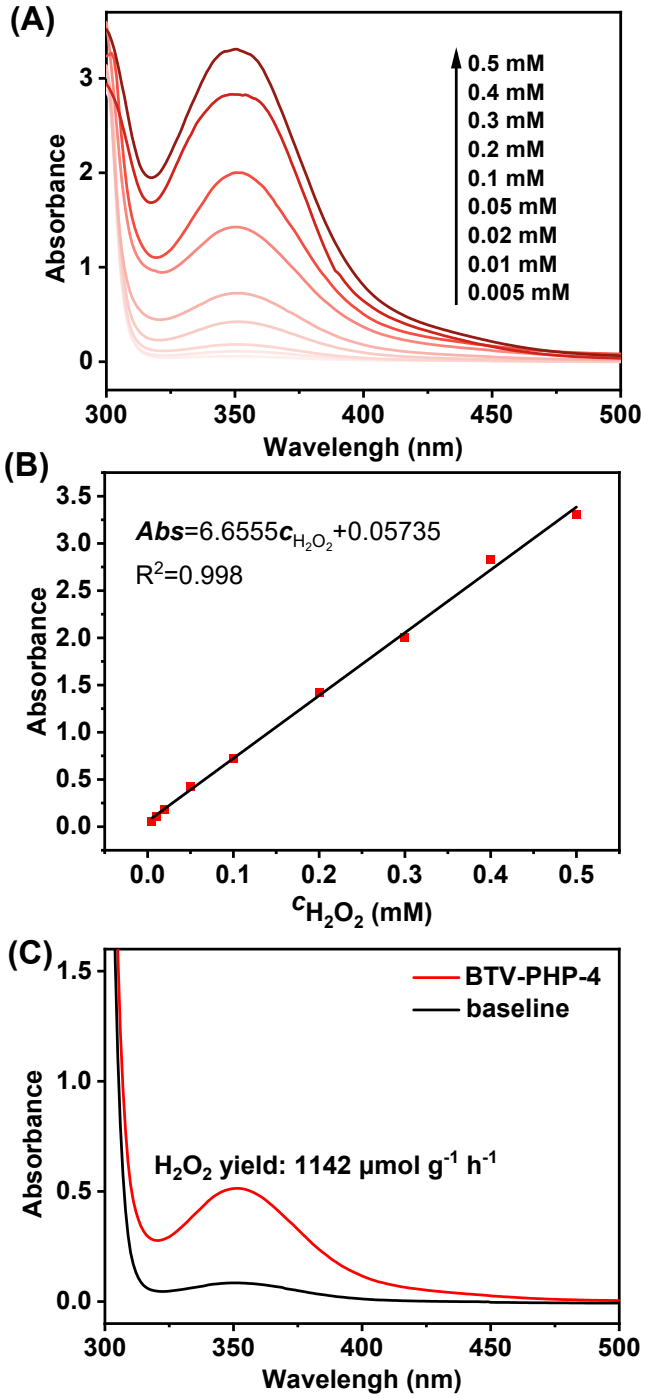

Fig. S25 Quantification of hydrogen peroxide (H_2O_2) generated during the photocatalytic reaction. (A) UV-Vis absorption spectra of various H_2O_2 concentrations measured by the iodometric method. (B) Calibration curve: linear fitting of absorbance versus standard H_2O_2 concentrations. (C) UV-Vis spectroscopy for H_2O_2 detection after reaction: the baseline represents the absorption of the pre-reaction mixture, and the red curve shows the absorption after 5 h of reaction over the photocatalyst BTV-PHP-4.

Determining the generation of H_2O_2 in the photocatalytic oxidative coupling of benzylamine

The quantification of H_2O_2 generated during the photocatalytic oxidative coupling of benzylamine was performed using a well-established iodometric method (Fig. S25). Specifically, 1 mL of 0.4 mol/L potassium iodide (KI) solution was mixed with 1 mL of 0.1 mol/L potassium hydrogen phthalate buffer solution. Then, 1 mL of the reaction supernatant—obtained by centrifuging the reaction mixture—was added to the mixture, which was then allowed to stand for 30 min. Under acidic conditions, H_2O_2 reacts completely with iodide ions to form triiodide (I_3^-), resulting in a color change from colorless to yellow. The reaction follows the equation: $H_2O_2 + 3I^- + 2H^+ \rightarrow 2H_2O + I_3^-$. The resulting solution was diluted 50-fold and analyzed by UV-Vis spectroscopy. The concentration of H_2O_2 was determined based on the absorbance at 350 nm, using a pre-established calibration curve for I_3^-.

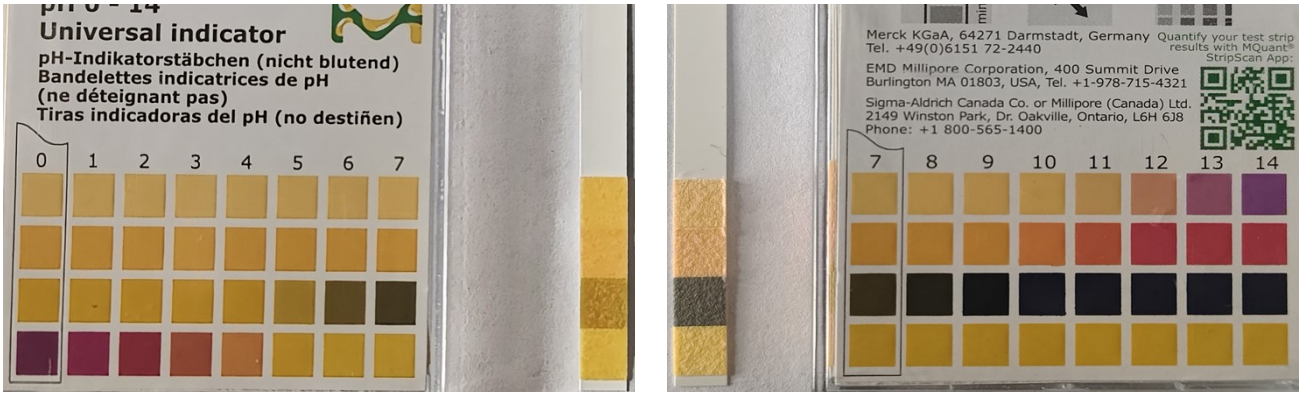

Before the reaction pH=5~6 During the reaction pH=7~8

Fig. S26 The pH test for the by-product NH_3-containing aqueous solution during the reaction.

The detection of ammonia (NH_3) generated during the photocatalytic oxidative coupling of benzylamine

Prior to the reaction, the pH of the distilled water used for absorption was measured and found to be 5–6 (Fig. S26, left). A mixture of benzylamine (0.5 mmol) and the photocatalyst BTV-PHP-4 (5 mg) was stirred under irradiation with blue LEDs at room temperature in air for 5 h, under solvent-free conditions. The NH_3 gas released during the reaction was continuously collected by bubbling the effluent gas into a test tube containing 3 mL of distilled water. The resulting aqueous solution was then extracted with dichloromethane (5 mL) to remove any potential interference from organic substrates such as benzylamine or imine products. The pH of the aqueous layer was subsequently measured and showed a distinct increase to 7–8 (Fig. S26, right), confirming the generation of NH_3 during the photocatalytic reaction.

Computational Details

All DFT calculations were carried out using ORCA (version: 5.0.3).[S28-S30] Geometry optimization was conducted at the r2SCAN-3c level of theory.[S31-S33] TD-DFT calculations were carried out at the PBE0/def2-SVP level on the structures after full geometric optimization.[S34,S35] A hole–electron analysis was implemented in Multiwfn, and the isosurface was visualized by VESTA software.[S34,S37]

References

S1 M. Mohamed, M. Hammad Elsayed, A. Hassan, A. Basit, I. Mekhemer, H. Chou, K. Chen and S.-K. Kuo, *ACS Appl. Polym. Mater.*, 2024, **6**, 5945.

S2 C. Hsiao, A. M. Elewa, M. G. Mohamed, M. G. Kotp, M. M.-C. Chou and S.-K. Kuo, *Colloid Surface A*, 2024, **699**, 134658.

S3 A. Basit, M. G. Mohamed, M. Ejaz, B. X. Su, H. Manzoor and S.-K. Kuo, *ACS Appl. Energy Mater.*, 2024, 7, 7505.

S4 M. G. Mohamed, M. H. Elsayed, Y. Ye, M. M. Samy, A. E. Hassan, T. H. Mansoure, Z. Wen, H.-H. Chou, K.-H. Chen, S.-W. Kuo, *Polymers*, 2023, 15, 182.

S5 X. Guo, J. Rabeah, R. Sun, D. Wang and E. Mejia, *ACS Appl. Mater. Interfaces*, 2021, **13**, 42889.

S6 M. Zhang and H. Liu, *ACS Appl. Polym. Mater*., 2025, **7**, 4633.

S7 Y. Zhang, N. Luo, J. Xu, K. Liu, S. Zhang, Q. Xu, R. Huang, Z. Long, M. Tong and G. Chen, *Dalton Trans*., 2020, **49**, 11300.

S8 S. Li, L. Li, Y. Li, L. Dai, C. Liu, Y. Liu, J. Li, J. Lv, P. Li and B. Wang, *ACS Catal*., 2020, **10**, 8717.

S9 S. Kumar, P. Chakrabortty, B. Banerjee, B. Kumbhakar, N. Siddiqui, S. Ghosh and S. Islam, *ACS Appl. Nano Mater.*, 2025, **8**, 12946.

S10 C.-Q. Han, J.-X. Guo, L. Wang, S. Sun, J. Lv, X. Sun, H. Hu, X. Huang and X.-Y. Liu, *J. Mater. Chem. C*, 2024, **12**, 16059.

S11 C.-Q. Han, Z.-Y. Wang, S. Sun, J.-X. Guo, X. Huang and X.-Y. Liu, *ACS Mater. Lett*., 2025, **7**, 393.

S12 Q. Li, J. Wang, Y. Zhang, L. Ricardez-Sandoval, G. Bai and X. Lan, *ACS Appl. Mater. Interfaces*, 2021, **13**, 39291.

S13 S. Jiang, X. Li, X. Zhang, Q. Ding and T. Cai, *J. Polym. Sci.*, 2024, **62**, 409.

S14 Z. Li, B. Cai, Y. Zou, D. Zhang, Y. Liang, Y. Zhou, Y. Ma, X. Wang, B. Shi, W.-K. Chen, Y. Liu and X. Zhao, *Adv. Energy Mater.*, 2025, **15**, 2500341.

S15 M. Yang, S. Zhang, M. Zhang, Z. Li, Y. Liu, X. Liao, M. Lu, S. Li and Y. Lan, *J. Am. Chem. Soc.*, 2024, **146**, 3396.

S16 X. Zeng, Q. Huang, X. Wang, J. Liu, M. Liu, G. Zhou, L. Zhao, J. Feng, C. Qian and Y. Liao, *Chin. J. Chem.*, 2025, **43**, 2885.

S17 L. Liu, W.-D. Qu, K.-X. Dong, Y. Qi, W.-T. Gong, G.-L. Ning and J.-N. Cui, *Chem. Commun.*, 2021, **57**, 3339.

S18 Z. Zhou, Z. Wang, A. L Blenko, J. Li and W. Lin, *J. Am. Chem. Soc*., 2025, **147**, 10846.

S19 Z. Xu, K. Liu, S. Wang, Y. Chang, J. Chen, S. Wang, C. Meng, Z. Long, Z. Qin and G. Chen, *ACS Appl. Polym. Mater.*, 2024, **6**, 701.

S20 C. He, P. Feng, L. Zhao and C. Duan, *Chem. Commun*., 2024, **60**, 4793.

S21 J. Kou, G. Wang, H. Guo, L. Li, J. Fang, J. Ma and Z. Dong, *Appl. Catal. B*, 2024, **352**, 124020.

S22 Z. Chen, J. Guo, F.-H. Song, S.-D. Wang, S. A. C. Carabineiro, S.-X. Ouyang and L.-L. Wen, *ACS Catal*., 2025, **15**, 8284.

S23 X. Liu, R. Qi, S. Li, W. Liu, Y. Yu, J. Wang, S. Wu, K. Ding and Y. Yu, *J. Am. Chem. Soc*., 2022, **144**, 23396.

S24 J. Chen, X. Chen, X. Cao, H. Ma, X. Jiang, Z. Sun and Y. Zhan, *J. Catal*., 2025, **446**, 116058.

S25 Mohit, K. Verma, A. Das and K. R. J. Thomas, *Langmuir*, 2025, **41**, 9800.

S26 S. Wang, J. Chen, Y. Chang, S. Wang, C. Meng, Z. Long and G. Chen, *J. Mater. Chem. A*, 2024, **12**, 14159.

S27 J. Chen, Y. Mao, Q. Shi, J. Yu, X. Bai, S. Wang, Z. Long and G. Chen, *J. Mater. Chem. A*, 2025, **13**, 33637.

S28 F. Neese, *Wiley Interdiscip. Rev.: Comput. Mol. Sci.*, 2012, **2**, 73.

S29 F. Neese, *Wiley Interdiscip. Rev.: Comput. Mol. Sci.*, 2018, **8**, e1327.

S30 F. Neese, *Wiley Interdiscip. Rev.: Comput. Mol. Sci.*, 2022, **12**, e1606.

S31 S. Grimme, A. Hansen, S. Ehlert and J.-M. Mewes, *J. Chem. Phys*., 2021, **154**, 064103.

S32 M. Gawron, F. Gilch, D. Schmidhuber, J. Kelly, T. Downie, A. Wangelin, J. Rehbein and R. Wolf, *Angew. Chem., Int. Ed.*, 2024, **63**, e202315381.

S33 J. Malenfant, L. Kuster, Y. Gagne, K. Signo, M. Denis, S. Canesi and M. Frenette, *Chem. Sci.*, 2024, **15**, 701.

S34 D. Mester and M. Kállay, *J. Chem. Theory Comput.*, 2022, **18**, 3, 1646.

S35 D. Mester and M. Kállay, *J. Chem. Theory Comput.*, 2022, **18**, 2, 865.

S36 T. Lu and F. Chen, *J. Comput. Chem.*, 2012, **33**, 5, 580.

S37 K. Momma and F. Izumi, *J. Appl. Crystallogr.*, 2011, **44**, 1272.